applied sciences

IMPACT FACTOR 2.5

CITESCORE 5.3

Article

Thermal Stability and Entropy Generation Analysis for Combustible Third-Grade Fluid Flow Through a Slant Channel: A Spectral Study

Kgomotshwana Frans Thosago, Peace Oluwalonimi Banjo, Lazarus Rundora and Samuel Olumide Adesanya

Special Issue

Research on Heat Transfer Analysis in Fluid Dynamics

Edited by

Dr. Pan Wang and Dr. Zhicheng Yuan

MDPI

https://doi.org/10.3390/app142411491

applied sciences

MDPI

Article

Thermal Stability and Entropy Generation Analysis for Combustible Third-Grade Fluid Flow Through a Slant Channel: A Spectral Study

Kgomotshwana Frans Thosago [1,*,†], Peace Oluwalonimi Banjo [2,†], Lazarus Rundora [1,†] and Samuel Olumide Adesanya [2,†]

[1] Department of Mathematics and Applied Mathematics, University of Limpopo, Private Bag X1106, Sovenga 0727, South Africa; lazarus.rundora@ul.ac.za
[2] Department of Mathematics and Statistics, Faculty of Natural Sciences, Redeemer's University, Ede 232101, Nigeria; banjop@run.edu.ng (P.O.B.); adesanyas@run.edu.ng (S.O.A.)
* Correspondence: frans.thosago@ul.ac.za; Tel.: +27-015-268-3351
† These authors contributed equally to this work.

Abstract: This paper addresses the mixed convective flow and heat transfer in combustible third-grade fluids through a slant porous channel filled with permeable materials. The fluid layer in contact with the channel wall is exposed to asymmetrical slippage and isothermal conditions. We employ the spectral Chebyshev collocation method (SCCM) to the coupled nonlinear flow governing equations and validate using the Shooting–Runge–Kutta method (RK4). Fluid velocity and temperature profiles, local entropy generation, and irreversibility ratio are computed and analyzed quantitatively and qualitatively. The convergence of the numerical method was demonstrated. The flow and thermal effects results, entropy generation rate, and Bejan number revealed fascinating manifestations that have profound implications in the design of thermo-mechanical systems. In particular, the thermal analysis results are pertinent to optimal system designs that achieve efficient energy utilization.

Keywords: reactive fluids; entropy generation; third-grade fluid; porous medium; variable viscosity; heat flux; fluid slippage

Citation: Thosago, K.F.; Banjo, P.O.; Rundora, L.; Adesanya, S.O. Thermal Stability and Entropy Generation Analysis for Combustible Third-Grade Fluid Flow Through a Slant Channel: A Spectral Study. *Appl. Sci.* **2024**, *14*, 11491. https://doi.org/10.3390/app142411491

Academic Editors: Pan Wang and Zhicheng Yuan

Received: 26 May 2024
Revised: 4 November 2024
Accepted: 4 December 2024
Published: 10 December 2024

1. Introduction

A good number of researchers have paid renewed interest and attention to the flow of reactive fluids because of their impact in technological advancements. In particular, energy transfer and the variable viscosity property of a fluid have been of vast interest among researchers [1–8]. Industrial and technological applications are found in areas such as atmospheric flows, thermal regulation, the cooling of electronic devices, nuclear reactors, thermal hydraulics, and many other devices have proliferated the engineering community. Meanwhile, entropy generation minimization in thermo-fluid flows is critically important in improving the efficiency of machines and processes, as explained by Bejan [9]. Therefore, efficient energy conversion and management is key in any thermal processes. In the industry, issues like productivity, sustainability, and competitiveness require engineering solutions, and such solutions are heavily reliant on mathematical models. Modern economies are being urged to curtail their energy dependence on fossil fuels in order to mitigate the continuous depletion of the ozone layer that is causing the acceleration of global warming. The deleterious consequences of global warming, like runaway fires, rising sea levels, and the melting of glaciers, are occurring at unsustainable rates in the present day. As more clean renewable energy forms are being sought to replace fossil fuels, it has become more and more urgent for economic systems to conserve more and more energy for continued sustainability. Thus, the need for continued research on entropy generation minimization cannot be over-emphasized. The assumption of the no-slip boundary condition has been the norm in most studies involving impervious and non-polished

surfaces. Many researchers are of the opinion that the no-slip boundary condition is a hypothesis. In fact, evidences of the slip of a fluid on a solid surface have been reported by several authors, including Mathews and Hill [10] and Zhu and Granick [11]. Ibáñez [12] and Nadeem and Akram [13] reported this effect on MHD flow in porous media and on the MHD peristaltic flow of a Jeffrey fluid, respectively. Das et al. [14] reported a magnetized flow with fluid slippage. The aim of this present study is to formulate a theoretical model, where we investigate the combined effects of slip, variable viscosity, porous-medium permeability, and channel porosity on entropy generation in the steady flow of a reactive third-grade fluid through an inclined channel filled with a porous saturated medium. A survey of the literature revealed that the scope of our study herein has not been fully accounted for in previous studies. Therefore, the main objective of this work is to present the thermal stability and entropy generation in the flow of combustible third-grade fluids with shear-induced slippage down a permeable channel filled with porous materials by using rapidly convergent spectral methods.

2. Mathematical Formulation

Consider the steady flow of an incompressible, variable-viscosity, reactive third-grade fluid through an inclined channel filled with a homogeneous and isotropic porous medium, as shown in Figure 1. The walls of the channel are assumed to be porous and to experience fluid slippage.

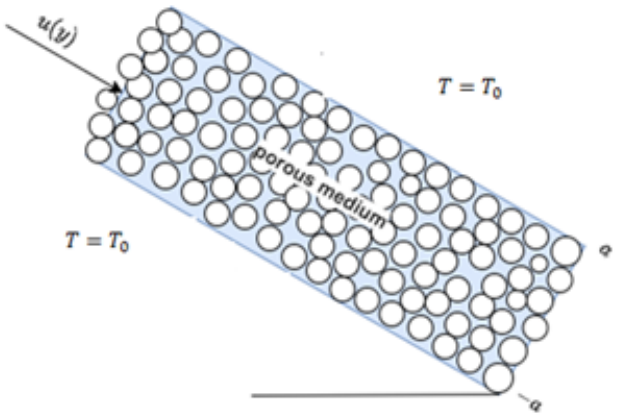

Figure 1. Schematic diagram of the problem.

The flow is assumed to be induced by an applied axial constant-pressure gradient and buoyancy force. Neglecting the reacting viscous fluid consumption, the model equations emanating from the momentum and heat balance can be written as [15]

$$\rho V_0 \frac{d\bar{u}}{d\bar{y}} = -\frac{d\bar{P}}{d\bar{x}} + \frac{d}{d\bar{y}}\left(\bar{\mu}(T)\frac{d\bar{u}}{d\bar{y}}\right) + 6\beta_3 \frac{d^2\bar{u}}{d\bar{y}^2}\left(\frac{d\bar{u}}{d\bar{y}}\right)^2 - \frac{\bar{\mu}(T)\bar{u}}{K} + \rho g\beta(T - T_0)sin(\omega), \quad (1)$$

$$\rho C_p V_0 \frac{d\bar{T}}{d\bar{y}} = k\frac{d^2T}{d\bar{y}^2} + \left(\frac{d\bar{u}}{d\bar{y}}\right)^2\left[\bar{\mu}(T) + 2\beta_3\left(\frac{d\bar{u}}{d\bar{y}}\right)^2\right] + \frac{\bar{\mu}(T)\bar{u}^2}{K} + QC_0A\left(\frac{hT}{vl}\right)^m e^{-\frac{E}{RT}}, \quad (2)$$

with appropriate boundary conditions

$$\left.\begin{aligned} \bar{y} = -a: \quad & \lambda_1\bar{u} = \mu(T)\frac{d\bar{u}}{d\bar{y}} + 2\beta_3\left(\frac{d\bar{u}}{d\bar{y}}\right)^3, \quad T = T_0 \\ \bar{y} = a: \quad & \lambda_2\bar{u} = -\mu(T)\frac{d\bar{u}}{d\bar{y}} + 2\beta_3\left(\frac{d\bar{u}}{d\bar{y}}\right)^3, \quad T = T_0 \end{aligned}\right\} \quad (3)$$

$\bar{P}$ is the modified fluid pressure, $\bar{x}$ and $\bar{y}$ are the axial and normal coordinates to the inclined channel, $\bar{u}$ is the fluid velocity, T_0 is the fluid initial temperature, T is the fluid temperature, g is the acceleration due to gravity, ω is the angle of inclination, β_3 is the third-grade material coefficient, k is the thermal conductivity, K is the porous-medium permeability, $\bar{\mu}$ is the fluid dynamic viscosity, ρ is the density, Q is the heat generated internally, C_0 is the initial concentration of the reactant species, A is the reaction rate constant, λ_1 and λ_2 are the slip coefficients at the lower and upper channel walls, respectively, E is the activation energy, h is the Boltzmann's constant, l is the Planck's number, R is the universal gas constant, ν is the vibration frequency, β is the volumetric thermal expansion coefficient, and m is the numerical exponent such that its three values represent numerical exponents for sensitized, Arrhenius, and bimolecular kinetics, respectively, as $m \in \{-2, 0, 0.5\}$ [16,17]. The temperature-dependent viscosity $\bar{\mu}(T)$ can be expressed as

$$\bar{\mu}(T) = \mu_0 e^{-b(T-T_0)} \tag{4}$$

where μ_0 is the initial fluid viscosity at temperature T_0 and b is the viscosity variation parameter. Introducing the following non-dimensional variables into Equations (1)–(4):

$$\left.\begin{array}{l} y = \dfrac{\bar{y}}{a},\ x = \dfrac{\bar{x}}{a},\ f = \dfrac{\bar{u}\rho a}{\mu_0},\ \alpha = \dfrac{bRT_0^2}{E},\ G = -\dfrac{dP}{dx},\ \Omega = \dfrac{\beta_3\mu_0}{\rho^2 a^4}, \\ Da = \dfrac{K}{a^2}, P = \dfrac{a^2\rho\bar{P}}{\mu_0^2}, \epsilon = \dfrac{RT_0}{E},\ \theta = \dfrac{E(T-T_0)}{RT_0^2}, \\ Gr = \dfrac{\rho^2 g\beta a^3 RT_0^2}{\mu_0^2 E},\ \gamma = \dfrac{\mu_0^3}{QA\rho^2 a^4 C_0}\left(\dfrac{\nu l}{hT_0}\right)^m e^{\frac{E}{RT_0}}, \delta^2 = \dfrac{1}{Da}, \\ \beta_1 = \dfrac{\mu_0}{\lambda_1 a},\ \beta_2 = \dfrac{\mu_0}{\lambda_2 a},\ Bi = \dfrac{ah_1}{k},\ \lambda = \dfrac{QEAa^2C_0}{kRT_0^2}\left(\dfrac{hT_0}{\nu l}\right)^m e^{-\frac{E}{RT_0}}, \end{array}\right\} \tag{5}$$

we obtain the non-dimensional governing equations

$$Ref' = e^{-\alpha\theta}f'' + 6\Omega f''f'^2 - \alpha e^{-\alpha\theta}f'\theta' - \delta e^{-\alpha\theta}f + Gr\theta Sin(\omega) + G, \tag{6}$$

$$RePr\theta' = \theta'' - \lambda\left((1+\epsilon\theta)^m exp\left(\frac{\theta}{1+\epsilon\theta}\right) + \gamma\left(f'^2\left(e^{-\alpha\theta} + 2\Omega f'^2\right) + \delta e^{-\alpha\theta}f^2\right)\right), \tag{7}$$

and we obtain the additional non-dimensional governing equations

$$\left.\begin{array}{ll} y = -1: & f = \beta_1\left[e^{-\alpha\theta}f' + 2\Omega(f')^3\right],\ \theta = 0 \\ y = 1: & f = -\beta_2\left[e^{-\alpha\theta}f' + 2\Omega(f')^3\right],\ \theta = 0 \end{array}\right\} \tag{8}$$

where Ω is the third-grade fluid material parameter, P is the fluid pressure, G is the pressure gradient, α is the variable viscosity parameter, ϵ is the activation energy parameter, Gr is the Grashof number, β_1, β_2 are the lower and upper wall slip parameters, respectively, Bi is the Biot number, Da is the Darcy number, δ is the porous-medium shape parameter, λ is the Frank-Kamenetsikii parameter, θ is the non-dimensional fluid temperature, x and y are the non-dimensional axial and normal coordinates to the inclined channel, and f is the non-dimensional fluid velocity.

3. Entropy Generation Analysis

The local volumetric rate of entropy generation for a viscous incompressible third-grade fluid in the presence of porous media is expressed as

$$E_G = \frac{k}{T_0^2}\left(\frac{d\bar{T}}{d\bar{y}}\right)^2 + \frac{\bar{\mu}(T)}{T_0}\left(\frac{d\bar{u}}{d\bar{y}}\right)^2\left(1 + \frac{2\beta_3}{\bar{\mu}(T)}\left(\frac{d\bar{u}}{d\bar{y}}\right)^2\right) + \frac{\bar{\mu}(T)\bar{u}^2}{KT_0}, \tag{9}$$

where the first term is the heat transfer irreversibility, the second term is the entropy generation due to third-grade fluid viscous dissipation, and the last term is the irreversibility due to the presence of porous media. Using the non-dimensional parameters and variables in (5), we obtain the equation for the non-dimensional entropy generation rate as

$$N_s = \theta'^2 + \frac{\lambda\gamma}{\epsilon} e^{-\alpha\theta}\left[f'^2(1 + 2\Omega e^{\alpha\theta} f'^2) + \delta f^2\right]. \tag{10}$$

The non-dimensional entropy generation number, $N_s = \frac{E_G a^2 E^2}{kR^2 T_0^2}$, is the ratio of the volumetric entropy generation rate to the characteristic entropy generation rate. Equation (10) can be expressed alternatively as

$$\left.\begin{aligned} N_s &= N_h + N_f, \\ N_h &= \theta'^2, \\ N_f &= \frac{\lambda\gamma}{\epsilon} e^{-\alpha\theta}\left[f'^2(1 + 2\Omega e^{\alpha\theta} f'^2) + \delta f^2\right], \end{aligned}\right\} \tag{11}$$

where N_h is the entropy generation due to heat transfer irreversibility and N_f is the entropy generation due to the combined fluid viscous dissipation and the porosity of the porous medium. The Bejan number (Be) is used to evaluate the irreversibility distribution and is defined as

$$Be = \frac{N_h}{N_h + N_f}. \tag{12}$$

According to Bejan [18], the Bejan number varies from 0 to 1, where $Be = 0$ tells us that the irreversibility due to fluid viscous dissipation and porosity dominate, whereas $Be = \frac{1}{2}$ indicates that the irreversibility due to fluid viscous dissipation and porosity is equal to the irreversibility due to heat transfer in the entropy production and $Be = 1$ reveals that the irreversibility due to heat transfer dominates.

4. Method of Solution

The system of nonlinear ordinary differential equations in (6) and (7), with the boundary conditions in (8), is solved numerically by the spectral Chebyshev collocation method (SCCM). Firstly, we assume trial polynomials of the form $\Psi_k(y)$:

$$\left.\begin{aligned} f(y) = f^N(y) &= \sum_{k=0}^{N} b_k \Psi_k(y), \\ \theta(y) = \theta^N(y) &= \sum_{k=0}^{N} c_k \Psi_k(y), \end{aligned}\right\} \tag{13}$$

Equation (13) is the spectral Chebyshev polynomial with the undetermined constants expected to satisfy (8). The residuals from (6) and (7) then become

$$\left.\begin{aligned} R_1 &= e^{-\alpha\theta^N} f_{yy}^N + 6\Omega f_{yy}^N f_y^{2N} - \alpha e^{-\alpha\theta^N} f_y^N \theta_y^N - \delta e^{-\alpha\theta^N} f^N + Gr\theta^N Sin(\omega) + G - Re f_y^N, \\ R_2 &= \theta_y^N y - \lambda\left((1 + \epsilon\theta^N)^m exp\left(\frac{\theta^N}{1 + \epsilon\theta^N}\right) + \gamma\left(f_y^{2N}\left(e^{-\alpha\theta^N} + 2\Omega f_y^{2N}\right) + \delta e^{-\alpha\theta^N} f^{2N}\right)\right) - RePr\theta_y^N, \end{aligned}\right\} \tag{14}$$

with boundary conditions

$$\left.\begin{aligned} y = -1: \quad f &= \beta_1\left[e^{-\alpha\theta^N} f_y^N + 2\Omega f_y^{3N}\right], \ \theta^N = 0 \\ y = 1: \quad f &= -\beta_2\left[e^{-\alpha\theta^N} f_y^N + 2\Omega f_y^{3N}\right], \ \theta^N = 0 \end{aligned}\right\} \tag{15}$$

The Gauss–Lobatto collocation points are given as

$$y_k = \left(-cos\left(\frac{i\pi}{N}\right)\right), \quad i = 0, 1, 2, ..., N \tag{16}$$

when solving for the algebraic system at

$$R_1(y_k) + R_2(y_k) = 0, \quad k = 0, 12, ..., 3 \tag{17}$$

Code Validation

The numerical solution from SCCM is then compared with the Shooting–Runge–Kutta method using NDSolve code since the validation of results is a major step in confirming the accuracy of numerical results. In this way, a simple Shooting–Runge–Kutta scheme is implemented by using the NDSolve algorithm in Wolfram Mathematica 13.3. The result is tabled against the SCCM results in Tables 1 and 2 for the parameter values $R = 0.1, \alpha = 0.1, \Omega = 0.1, \delta = 0.1, Gr = 0.1, m = 0.5, \gamma = 0.1, \beta_1 = 0.1, \beta_2 = 0.1, \psi = 0.1, Pr = 1, \lambda = 0.1, \epsilon = 0.1$.

Table 1. Validation for the solution of $f(y)$.

y	$f(y)_{SCCM}$	$f(y)_{RK4}$	$\lvert f(y)_{SCCM} - f(y)_{RK4} \rvert$
−1.0	0.09340042731013098	0.0934004275457099	$2.355789174846023 \times 10^{-10}$
−0.75	0.2782702518827663	0.2782702628881371	$1.100537083686958 \times 10^{-8}$
−0.5	0.41810875686198196	0.41810878741114443	$3.054916247746675 \times 10^{-8}$
−0.25	0.5073637119780844	0.5073637713586425	$5.93805581372564 \times 10^{-8}$
0.0	0.5408032211708456	0.5408032769405969	$5.576975137255857 \times 10^{-8}$
0.25	0.515175556370712	0.5151755848661947	$2.849548275118962 \times 10^{-8}$
0.5	0.4305925030480927	0.4305925270588788	$2.401078608160745 \times 10^{-8}$
0.75	0.29025067501405133	0.2902507313095687	$5.629551735886196 \times 10^{-8}$
1.0	0.09886799791001163	0.09886808703206998	$8.91220583443264 \times 10^{-8}$

Table 2. Validation for the solution of $\theta(y)$.

y	$\theta(y)_{SCCM}$	$\theta(y)_{RK4}$	$\lvert \theta(y)_{SCCM} - \theta(y)_{RK4} \rvert$
−1.0	$1.1006285586 \times 10^{-19}$	0.0	$1.100628558680762 \times 10^{-19}$
−0.75	0.02272084331322944	0.02272084285202028	$4.612091611400082 \times 10^{-10}$
−0.5	0.039238086997582716	0.0392380865496249	$4.479578166738385 \times 10^{-10}$
−0.25	0.049427524412263134	0.049427523946807654	$4.654554797145494 \times 10^{-10}$
0.0	0.05315385368892104	0.053153853296836195	$3.920848437588553 \times 10^{-10}$
0.25	0.05026408527117134	0.050264085011262935	$2.599084072962831 \times 10^{-10}$
0.5	0.04058133464454575	0.04058133447864745	$1.658982951013854 \times 10^{-10}$
0.75	0.023902559552278567	0.023902559431809665	$1.204689022149541 \times 10^{-10}$
1.0	$1.4543862558 \times 10^{-18}$	$-1.412512538815998 \times 10^{-11}$	$1.412512684254624 \times 10^{-11}$

5. Results

Computational results from Tables 1 and 2 revealed that the two numerical results converged to the same solution. Table 3 shows that the SCCM converges very fast with few approximations. The stability analysis results in Table 4 revealed that the third-grade fluid parameter, activation energy, suction, and Prandtl number delay the occurrence of thermal explosion, while the porous-medium shape and viscosity variation parameters lead to the early occurrence of thermal instability. The combined effects of temperature-dependent viscosity, porous media permeability, slip, and suction and injection on the flow of a reactive third-grade fluid in an inclined channel have been studied. In the following discussion, we carry out a detailed thermodynamic analysis of the dependence of the fluid velocity and temperature profiles, the entropy generation, and the irreversibility ratio on the various thermophysical parameters embedded in the flow system. We present the SCCM graphical solutions and provide a qualitative description of the simulated variations. Unless otherwise stated, the following parameter values are employed. Where a parameter is not varied, these are the default values used: $\psi = 0.1, \beta_2 = 0.1, Re = 0.1, Pr = 1, \epsilon = 0.1, \alpha = 0.1, m = 0.5, \beta_1 = 0.3, Np = 40, \lambda = 0.1, \Omega = 0.1, \delta = 0, Gr = 0.1$.

Table 3. Convergence for $R = 0.1, \delta = 0.1, Gr = 0.1, \psi = 0.1, \epsilon = 0.1, \beta_1 = 0.1, \beta_2 = 0.1$.

N	α	Ω	γ	Pr	m	λ_c	Nu
5	0.1	0.1	0.1	1	0.5	0.9279092917369934	2.508861980241903
10	0.1	0.1	0.1	1	0.5	0.9265627889759518	2.5127667585340197
15	0.1	0.1	0.1	1	0.5	0.9265626198294173	2.512743597875568
20	0.1	0.1	0.1	1	0.5	0.9265626198037284	2.512743516672778
25	0.1	0.1	0.1	1	0.5	0.9265626197961245	2.512743516672778
30	0.1	0.1	0.1	1	0.5	0.9265626197960075	2.5127435251789016

Table 4. $N = 25$ thermal criticality.

Ω	ϵ	Re	δ	α	Pr	λ_c
0.1	0.1	0.1	0.1	0.1	1	0.9265626197961245
0.3	1	0.1	0.1	0.1	1	0.9272038629192019
0.5	1	0.1	0.1	0.1	1	0.9275992070933973
0.1	0.2	0.1	0.1	0.1	1	0.9968642284351334
0.1	0.3	0.1	0.1	0.1	1	1.1010602941629342
0.1	0.1	0.2	0.1	0.1	1	0.9290721522005858
0.1	0.1	0.3	0.1	0.1	1	0.9332508140705013
0.1	0.1	0.1	0.5	0.1	1	0.9262095529877397
0.1	0.1	0.1	0.8	0.1	1	0.9262037341789104
0.1	0.1	0.1	0.1	0.3	1	0.9247410643800902
0.1	0.1	0.1	0.1	0.5	1	0.9227470150928092
0.1	0.1	0.1	0.1	0.1	2	0.929043675503623
0.1	0.1	0.1	0.1	0.1	3	0.9331744078741027

5.1. Velocity Profile

The response of the fluid velocity profile to the various flow parameters is displayed in Figures 2–8. The figures reveal parabolic velocity profiles, where the maximum velocity is recorded at the center of the channel. Figure 2 shows the influence of the viscosity variation

parameter on the flow velocity. As the plot shows, when the viscosity parameter increases, the fluid's dynamic viscosity increases. This is explained by the fact that increasing the parameter α means that the fluid's viscosity is reduced, leading to diminished resistance to flow. This inevitably leads to increased fluid velocity. Figure 3 shows the influence of the viscous heating parameter on the flow velocity. From the plot, when the viscous dissipation parameter rises, the magnitude of the heat generated within the flow domain increases accordingly; hence, the flow velocity is enhanced, as seen in the figure. Figure 4 shows that the activation energy parameter ϵ has little or no significant effect on the fluid velocity. This is explained by the fact that the activation energy parameter implicitly enters the velocity equation through the temperature/viscosity coupling. In this way, its effects on the velocity can, at best, be marginal. An increase in the Grashof number Gr, Figure 5, is observed to increase the fluid velocity. Variations in the Grashof number explain the buoyancy effects on the flow. Higher Grashof numbers point to increased buoyancy source terms, which result in the corresponding increase in the fluid velocity, as illustrated in Figure 5. The variation of the fluid velocity in response to increasing values of the Frank-Kamenetsikii parameter (chemical reaction parameter λ) is displayed in Figure 6. An increase in the chemical reaction parameter means that the rate of chemical reaction increases, and so do the heating source terms. Therefore, flow velocity is expected to increase in the flow channel. Figures 7 and 8 show the flow-damping effects of the third-grade material parameter and the porous-medium shape parameter δ, respectively. An increase in the third-grade material parameter Ω results in corresponding increases in the non-Newtonian properties of the fluid, like the visco-elastic effects and others that induce increased resistance to flow. On the other hand, increasing the porous-medium shape parameter means that the pore spaces in the porous matrix are reduced, resulting in reduced porosity and damping the flow.

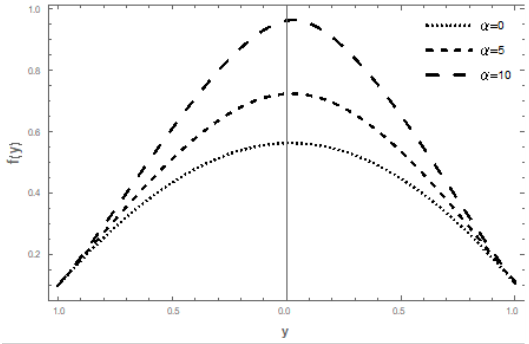

Figure 2. Variation of the velocity profile with a variable viscosity parameter.

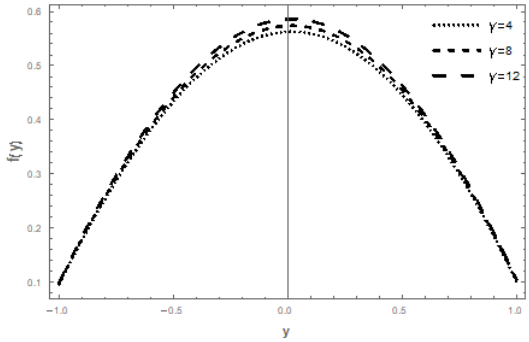

Figure 3. Variation of the velocity profile with a viscous heating parameter.

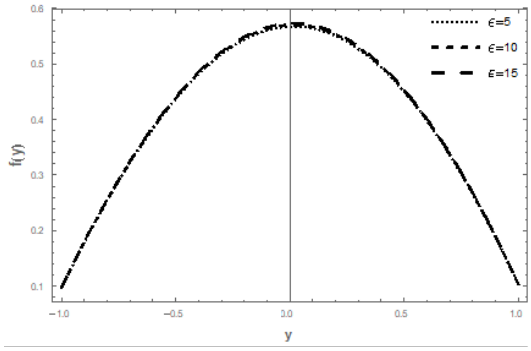

Figure 4. Variation of the velocity profile with the activation energy parameter.

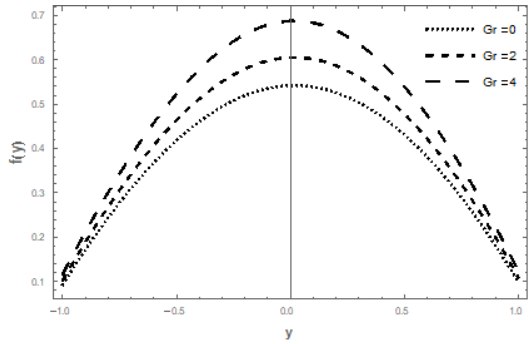

Figure 5. Variation of the velocity profile with the Grashof number.

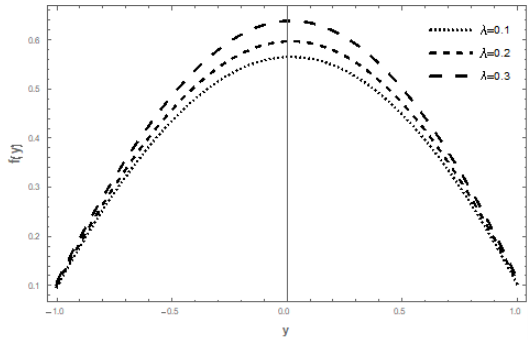

Figure 6. Variation of the velocity profile with the Frank-Kamenetskii parameter.

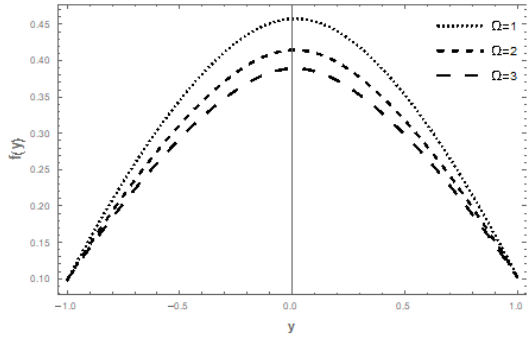

Figure 7. Variation of the velocity profile with the third-grade material parameter.

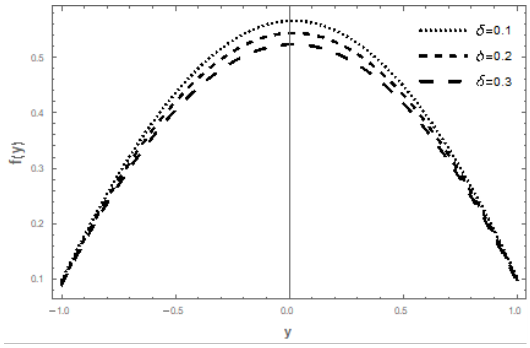

Figure 8. Variation of the shape factor parameter velocity profile with porous medium.

5.2. Fluid Temperature Distribution

Figures 9–15 display the variations of the fluid temperature profile in response to various flow-governing parameters. Except for Figure 15, where the third-grade material parameter retards the fluid temperature, all the other figures show the fluid temperature increasing with an increase in the values of the variable viscosity parameter, the viscous heating parameter, the activation energy parameter, the Grashof number, the chemical reaction parameter, and the porous-medium shape parameter. The viscous heating and the chemical reaction parameters are observed to cause the most significant increase in fluid temperature. As alluded to earlier in the discussion, the increasing values of the variable viscosity parameter mean that the fluid viscosity is reduced, diminishing the fluid's resistance to flow. The resultant increased fluid velocity increases the viscous heating source terms in the temperature equation, leading to the elevation of fluid temperature, as depicted in Figure 9. In Figure 10, the viscous heating parameter, a measure of heat source from the core of the channel, is observed to increase the fluid temperature significantly, as pointed to earlier. In Figure 11, the fluid velocity profile is enhanced by an increase in the activation energy parameter. In Figure 12, increasing buoyancy forces lead to an increase in fluid temperature. The heat source from the channel core region into the fluid leads to a volumetric thermal expansion, which induces some overturning instability in the fluid that causes the fluid particles to move faster. Due to coupling, the increased velocity increases the heating source terms in the temperature equation, resulting in enhanced fluid temperature. Figure 13 shows that the fluid temperature increases significantly with an increase in the values of the chemical reaction parameter. This phenomenon is explained earlier, in Section 5.1. Section 5.1 explains the reduction of fluid velocity due to increasing non-Newtonian character as measured by the third-grade material parameter. The reduced velocity, in turn, decreases the viscous heating source terms in the temperature equation, which leads to a drop in fluid temperature, as shown in Figure 14. In Figure 15, except very close to the isothermal walls, elsewhere in the channel, an increase in the porous-medium shape parameter values causes a slight increase in the fluid temperature. This can be attributed to the frictional forces caused by the fluid particles as they force their way into reduced pore spaces.

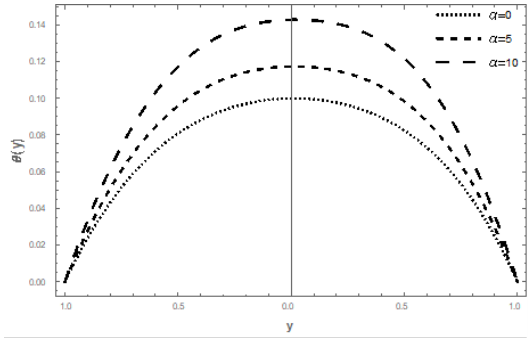

Figure 9. Variation of the temperature distribution with a variable viscosity parameter.

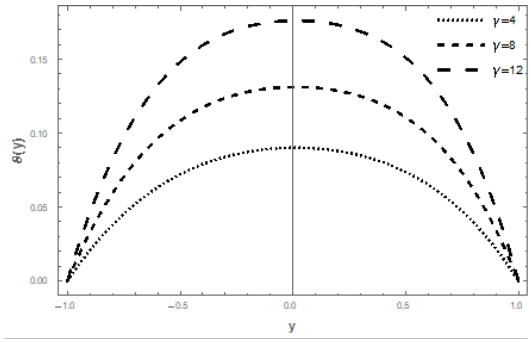

Figure 10. Variation of the temperature distribution with the viscous heating parameter.

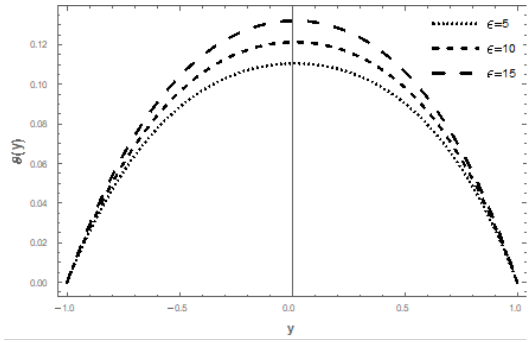

Figure 11. Variation of the temperature distribution with the activation energy parameter.

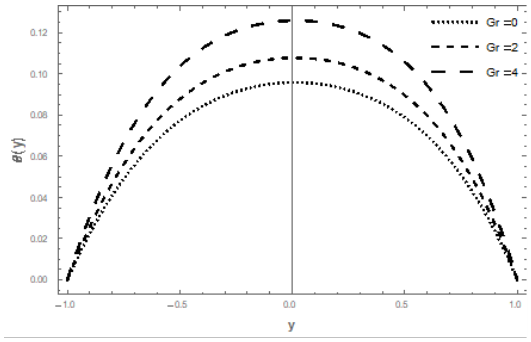

Figure 12. Variation of the temperature distribution with the Grashof number.

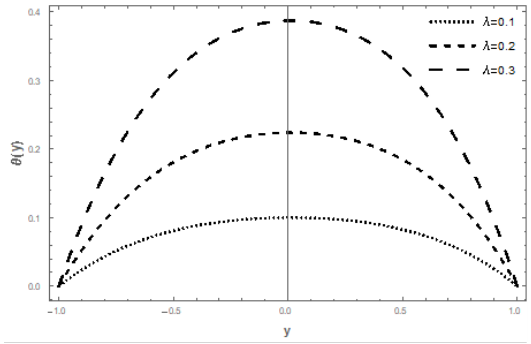

Figure 13. Variation of the temperature distribution with the Frank-Kamenetskii parameter.

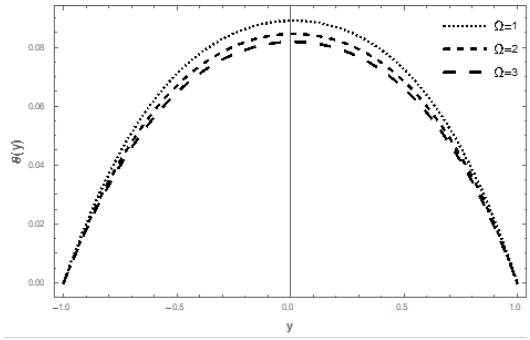

Figure 14. Variation of the temperature distribution with the third-grade material parameter.

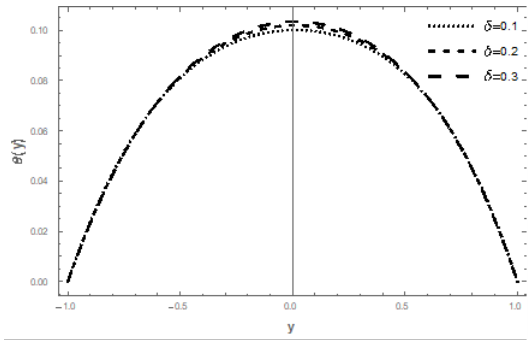

Figure 15. Variation of the temperature distribution with the porous-medium shape parameter.

5.3. Entropy Generation

The entropy generated in the flow is analyzed using Figures 16–22. The figures depict parabolic entropy profiles with minimum entropy rate Ns = 0 at the channel core region. Figures 16, 17 and 19 show the entropy generation rate increasing with increasing values of the variable viscosity parameter, the viscous heating parameter and the Grashof number, respectively. In Figure 19, the entropy generation rate increases throughout the entire channel, including the core region. Figures 18 and 21 depict the entropy generation rate decreasing with the activation energy parameter and the third-grade material parameter throughout the entire channel, including the core region. In Figure 20, the Frank-Kamenetsikii parameter is seen to enhance the entropy generation rate in the entire channel. In the core region of the channel, as seen in Figure 22, an increase in the porous-medium shape parameter enhances the entropy generation rate, while, at the channel walls, the entropy generation rate decreases.

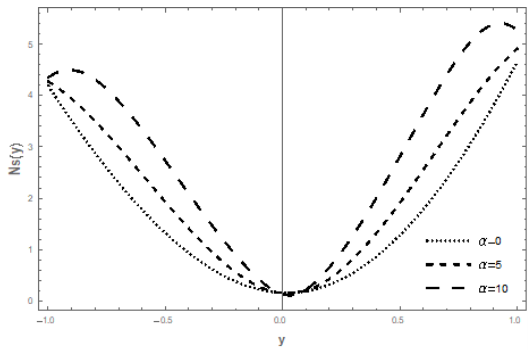

Figure 16. Variation of the entropy generation with a variable viscosity parameter.

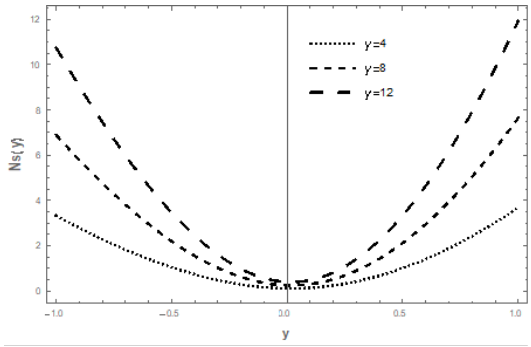

Figure 17. Variation of the entropy generation with the viscous heating parameter.

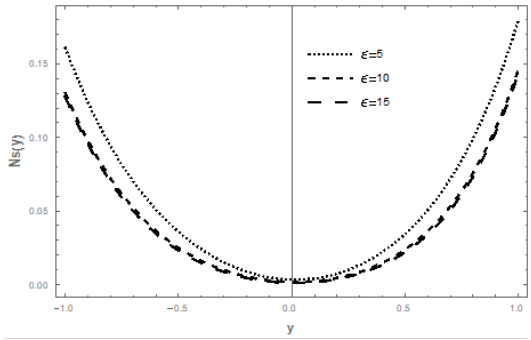

Figure 18. Variation of the entropy generation with the activation energy parameter.

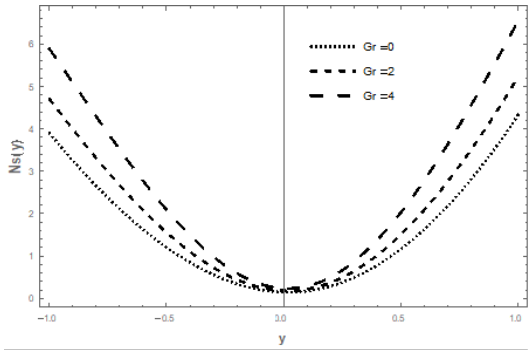

Figure 19. Variation of the entropy generation with the Grashof number.

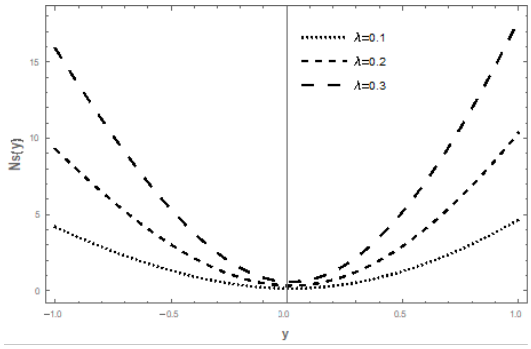

Figure 20. Variation of the entropy generation with the Frank-Kamenetsikii parameter.

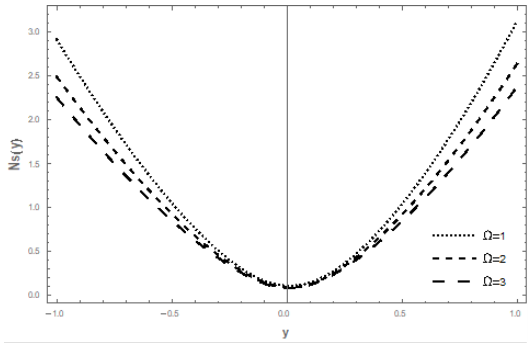

Figure 21. Variation of the entropy generation with the third-grade material parameter.

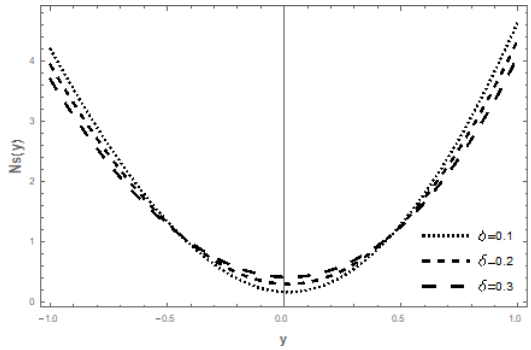

Figure 22. Variation of the entropy generation with the porous-medium shape parameter.

5.4. Bejan Number

Figures 23–29 demonstrate the irreversibility ratio trends in response to variations in the flow governing parameters. A striking feature of all seven graphs is that the irreversibility ratio is minimal at the core region of the channel. This shows that, in this flow, irreversibility due to the combined effect of viscous dissipation and porous-medium permeability attains its maximum value at the channel core region while it weakens at the channel walls. Figures 23, 24 and 26 show that, with the increasing variable values of the viscosity parameter, viscous heating, and Grashof number, there is a perfect dominance of irreversibility due to heat transfer over irreversibility due to the combined effect of viscous dissipation and porous-medium permeability in the bulk of the fluid and closer to the channel walls. However, we noted that, at the channel core region, this dominance is weakened by viscous dissipation and porous-medium permeability irreversibility, as can be seen from the magnitude of the Bejan number. An interesting observation in Figure 25 is that the irreversibility ratio is constant at $y = 0$ in the channel core region except around the walls, where heat transfer irreversibility is significant. Also, in Figure 25, increasing activation energy parameter values elevate the channel's Bejan number. The effects of the Grashof number on the irreversibility ratio, Figure 26, mirror those of the viscous heating parameter, albeit at a less pronounced intensity. In Figure 27, an increase in the chemical reaction parameter reveals effects that are like the impact of the activation energy parameter described in Figure 25. In Figure 28, an increase in the fluid's non-Newtonian properties has negligible effects on the Bejan number, showing only a marginal increase in the bulk of the fluid. The third-grade material parameter contributes more to the viscous dissipation and porous-medium permeability irreversibility in the flow channel. Similar behavior is seen in Figure 29 for increasing porous-medium shape parameter values.

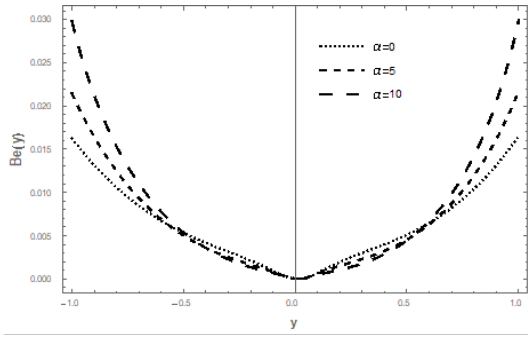

Figure 23. Variation of the Bejan number with a variable viscosity parameter.

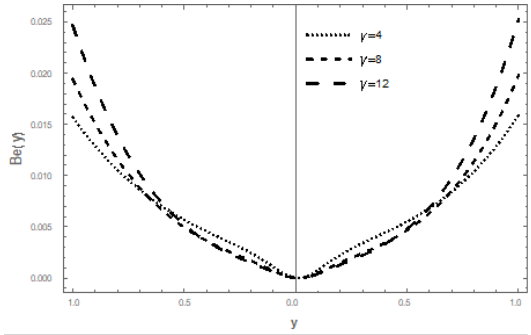

Figure 24. Variation of the Bejan number with the viscous heating parameter.

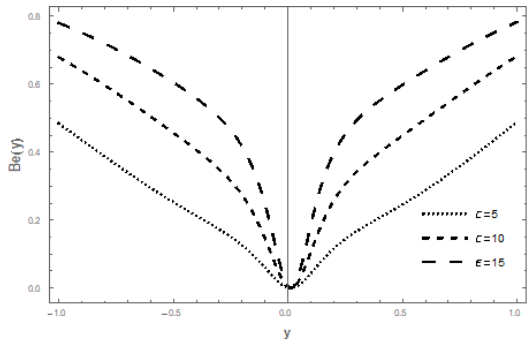

Figure 25. Variation of the Bejan number with the activation energy.

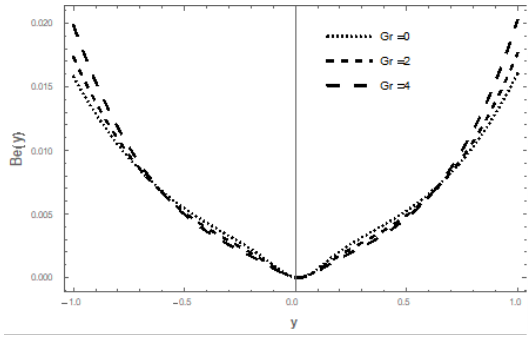

Figure 26. Variation of the Bejan number with the Grashof number.

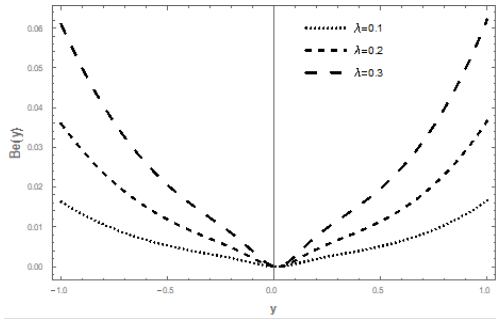

Figure 27. Variation of the Bejan number with the Frank-Kamenetsikii parameter.

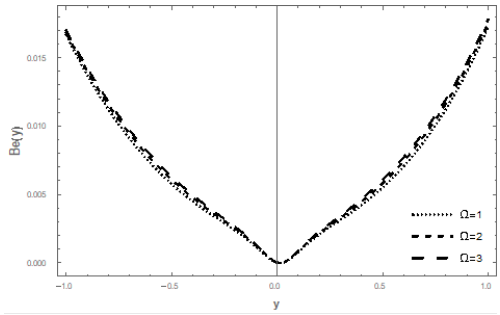

Figure 28. Variation of the Bejan number with the third-grade material parameter.

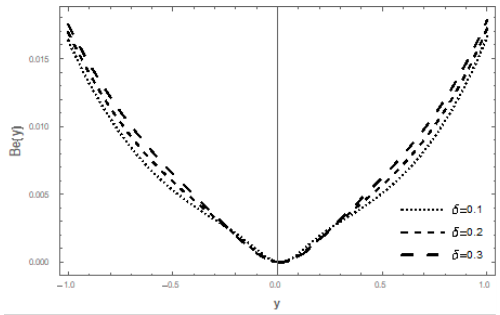

Figure 29. Variation of the Bejan number with the porous-medium shape factor parameter.

5.5. Thermal Criticality

The bifurcation slice reveals that the solution branches are just like every other combustion. The problem has one solution from the plot in Figure 30, at the thermal critical value $\lambda_c = 0.926562619796$, $Nu = 2.51274351668$. Beyond this critical value, the solution does not exist, while the problem has two solutions below the critical value.

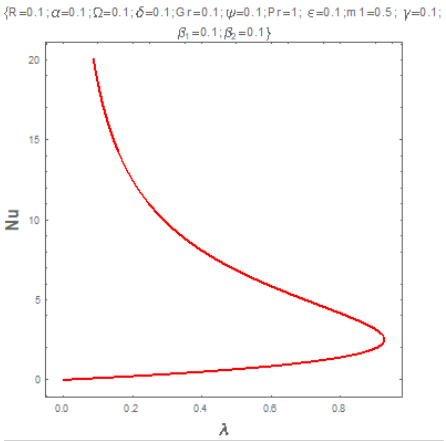

Figure 30. Thermal criticality bifurcation plot.

6. Conclusions

In this article, the entropy generation analysis of a steady flow of a reactive variable-viscosity third-grade fluid through a slant porous-medium saturated channel with asymmetrical slippage and isothermal conditions was successfully carried out with the aid of SCCM. The numerical method was found to be highly accurate and convergent. A graphical analysis of the response of the velocity and temperature distribution, entropy generation rate, and irreversibility ratio to the various parameters embedded in the flow system revealed the following:

- The non-Newtonian properties of the fluid and the porous-medium shape factor parameter have a damping effect on the fluid velocity, while the buoyancy forces were observed to have the opposite effect;
- The fluid temperature profile was observed to increase with an increase in the temperature-dependent viscosity, the viscous heating parameter, the activation energy parameter, the buoyancy force, and the chemical reaction parameter, whereas the third-grade material parameter had a retardation effect;
- A parabolic entropy generation rate profile was observed, with minimum entropy $Ns = 0$ at the channel core region;
- Parameters either increase or decrease the entropy generation rate elsewhere in the channel, but, at the core region of the channel, it remained unaffected by all the parameters except the chemical reaction parameter, the activation energy parameter, buoyancy, and porous-medium permeability;
- The irreversibility ratio was observed to be minimum at the channel core region, indicating the dominance of the combined viscous dissipation and porosity irreversibility over heat transfer irreversibility;
- Elsewhere in the channel, parameters revealed varied effects on the Bejan number but, in general, irreversibility due to viscous dissipation and porosity was found to dominate heat transfer irreversibility at the core region of the channel. Heat transfer irreversibility was, in general, dominant near the channel walls and in the bulk of the fluid further from the core region. These observed interesting manifestations will no doubt inform optimal system regulation criteria for entropy generation minimization in thermo-mechanical systems to achieve energy utilization efficiency.

There is growing demand for economical and maintainable systems across the globe. Most industrial and engineering flow processes and thermal systems are unable to work at optimal levels due to entropy generation. Since entropy generation is a measure of the destruction of the accessible work of the systems, the determination of entropy generation is thus extremely vital for upgrading system performance. Our study is a theoretical model through which the factors (or parameters) that contribute to entropy generation can be identified so that their effects can be minimized through intelligent regulation so that the flow system efficiency can be maximized. Moreover, with the global technological advancements of non-Newtonian fluids, the theoretical results will provide guidance on improving, conserving, and upgrading several designs in industrial thermo-fluid systems.

Author Contributions: Conceptualization, L.R.; methodology, P.O.B.; software, S.O.A.; validation, P.O.B.; formal analysis, K.F.T.; writing, L.R.; review and editing, S.O.A.; funding acquisition, K.F.T. All authors have read and agreed to the published version of the manuscript.

Funding: This research received no external funding.

Institutional Review Board Statement: Not applicable.

Informed Consent Statement: Not applicable.

Data Availability Statement: The raw data supporting the conclusions of this article will be made available by the authors on request.

Conflicts of Interest: The authors declare no conflicts of interest

Abbreviations

The following abbreviations are used in this manuscript:

RK4	Shooting–Runge–Kutta method
SCCM	Spectral Chebyshev Collocation Method

References

1. Thosago, K.F.; Rundora, L.; Adesanya, S.O. Thermodynamic analysis of magnetohydrodynamic third grade fluid flow with variable properties. *Int. J. Eng. Res. Afr.* **2021**, *55*, 28–46. [CrossRef]
2. Ellahi, R.; Riaz, A. Analytical solutions for MHD flow in a third-grade fluid with variable viscosity. *Math. Comput. Model.* **2010**, *52*, 1783–1793. [CrossRef]
3. Adesanya, S.O.; Rundora, L.; Thosago, K.F. Numerical evaluation of heat irreversiblity in porous medium combustion of third-grade fluid subjected to Newtonian cooling. *Numer. Heat Transf. Part A Appl.* **2023**, *84*, 1091–1105. [CrossRef]
4. Akinshilo, A.T. Steady flow and heat transfer analysis of third grade fluid with porous medium and heat generation. *Eng. Sci. Technol. Int. J.* **2017**, *20*, 1602–1609. [CrossRef]
5. Okoya, S.S. Computational study of thermal influence in axial annular flow of a reactive third grade fluid with non-linear viscosity. *Alex. Eng. J.* **2019**, *58*, 401–411. [CrossRef]
6. Makinde, O. Irreversibility analysis of variable viscosity channel flow with convective cooling at the walls. *Can. J. Phys.* **2008**, *86*, 383–389. [CrossRef]
7. Makinde, O. Entropy-generation analysis for variable-viscosity channel flow with non-uniform wall temperature. *Appl. Energy* **2008**, *85*, 384–393. [CrossRef]
8. Mondal, H.; Mishra, S.; Kundu, P.K.; Sibanda, P. Entropy Generation of Variable Viscosity and Thermal Radiation on Magneto Nanofluid Flow with Dusty Fluid. *J. Appl. Comput. Mech.* **2020**, *6*, 171–182.
9. Bejan, A. Second law analysis in heat transfer. *Energy* **1980**, *5*, 720–732. [CrossRef]
10. Matthews, M.; Hill, J. Newtonian flow with nonlinear Navier boundary condition. *Acta Mech.* **2007**, *191*, 195–217. [CrossRef]
11. Zhu, Y.; Granick, S. Rate-dependent slip of Newtonian liquid at smooth surfaces. *Phys. Rev. Lett.* **2001**, *87*, 096105. [CrossRef] [PubMed]
12. Ibáñez, G. Entropy generation in MHD porous channel with hydrodynamic slip and convective boundary conditions. *Int. J. Heat Mass Transf.* **2015**, *80*, 274–280. [CrossRef]
13. Nadeem, S.; Akram, S. Slip effects on the peristaltic flow of a Jeffrey fluid in an asymmetric channel under the effect of induced magnetic field. *Int. J. Numer. Methods Fluids* **2010**, *63*, 374–394. [CrossRef]
14. Das, S.; Jana, R. Entropy generation in an unsteady MHD channel flow with Navier slip and asymmetric convective cooling. *Int. J. Ind. Math.* **2017**, *9*, 149–160.
15. Salawu, S.O.; Fatunmbi, E.O. Inherent irreversibility of hydromagnetic third-grade reactive poiseuille flow of a variable viscosity in porous media with convective cooling. *J. Serbian Soc. Comput. Mech.* **2017**, *11*, 46–58. [CrossRef]
16. Frank-Kamenetskii, D.A. *Diffusion and Heat Transfer in Chemical Kinetics*; Plenum Press: New York, NY, USA, 1969.
17. Makinde, O.D. Thermal stability of a reactive viscous flow through a porous-saturated channel with convective boundary conditions. *Appl. Therm. Eng.* **2009**, *29*, 1773–1777. [CrossRef]
18. Bejan, A. Entropy generation minimization: The new thermodynamics of finite-size devices and finite-time processes. *J. Appl. Phys.* **1996**, *79*, 1191–1218. [CrossRef]